Topological Hall Effect in Bi/Cr_2Te_3 Heterostructure Thin Films

Zijun Yan[1,2], Wenyu Hu[1], Liang Zhou[1], Xinru Han[1], Jie Jiang[1], Hangyu Yin[1], Yang Qiu[3], Hongtao He[1], Shu Ping Lau[2*], Gan Wang[1,4*]*

[1]Department of Physics, Southern University of Science and Technology, Shenzhen 518055, China

[2]Department of Applied Physics, the Hong Kong Polytechnic University 100872, Hong Kong, China

[3]Materials Characterization and Preparation Center, Southern University of Science and Technology, Shenzhen 518055, China

[4]Shenzhen Institute for Quantum Science and Engineering, and Department of Physics, Southern University of Science and Technology, Shenzhen 518055, China

Keywords: Bi, Cr_2Te_3, Topological Hall Effect, Molecular beam epitaxy

Abstract: The topological Hall effect (THE) due to the spatially varying magnetizations appears as humps and dips near the coercive field in the Hall resistance curves. It is possible evidence of magnetic skyrmions that might be applied to next-generation data storage devices. Previous calculation predicted that the combination of Cr_2Te_3 thin film with strong perpendicular anisotropy (PMA) and Bi with strong spin-orbital coupling (SOC) could induce Dzyaloshinskii-Moriya Interaction (DMI) and magnetic skyrmions. THE has been observed in Cr_2Te_3 thin films with Bi bilayer nanosheets intercalated. However, the distribution of inserted Bi nanosheets was random, so locating and

studying the interface between Bi and Cr_2Te_3 layers is difficult. The growth scheme of Bi on Cr_2Te_3 surface is still blank. In this work, Bi/Cr_2Te_3 heterostructure thin films were fabricated by molecular beam epitaxy (MBE). Bi (1 1 0) surface was grown on the Cr_2Te_3 (0 0 0 1) layer in islands from cross-sectional and plane-view scanning transmission electron microscopy (STEM) observation. THE signals were observed in the Bi/Cr_2Te_3 heterostructure thin films below 130 K. The two-component anomalous Hall effect (AHE) that might induce similar hump and dip signals near the coercive field was excluded by the minor-loop method.

1. Introduction

Topological Hall effect (THE) was proposed by Bruno *et al.* to describe the Hall effect that only depends on the topology of magnetization texture in the sample without an external magnetic field in 2004[1]. Nontrivial spin textures are necessary for the generation of THE. An electron will adiabatically follow the local magnetization direction during its motion in a two-dimensional material with a spatially varying magnetization. It will pick up the Berry phase[2] after this process and attain a transverse velocity which induces additional Hall current, which will yield a hump or a dip near the coercive field in the Hall resistance curves[1]. The spatially varying magnetizations include topological states such as magnetic skyrmions, spin chirality on Kagome, and chiral (right- and left-handed) domain walls[3]. Thus, it can be observed in abundant materials subjected to topological phases and topological spin texture, especially magnetic skyrmions. For example, THE was already produced in antiferromagnetic Dirac semimetal EuAgAs[4], MnP with spin chirality[5], WTe_2/Fe_3GeTe_2 heterostructure with Neel-type skyrmion[6], Ferromagnet Fe_3GeTe_2 with Bloch-type skyrmion[7] and so on. Skyrmions were introduced in field theory by physicist Tony Skyrme to describe a localized, particle-like configuration[8], and their formation in a magnetic system was predicted theoretically several decades later[9]. The magnetic skyrmions are topologically protected vortex-like nanometric spin textures[10]. They have recently received growing attention for their potential applications as information carriers in

magnetic information storage and processing devices. THE was observed in some intrinsic Cr-Te compound thin films such as Cr_3Te_4 due to biskyrmions[11], Cr_5Te_6 due to noncoplanar spin textures[12], $Cr_{0.87}Te$ due to magnetic skyrmionic bubbles[13]. In addition, the interface between some Cr-Te compound thin film without THE and other materials with spin-orbit coupling (SOC) (e.g., $CrTe/SrTiO_3$[14] and $CrTe_2/Bi_2Te_3$[15]) might generate Dzyaloshinskii-Moriya Interaction (DMI), and THE would be induced in the heterostructure system. Besides, in previous research[16, 17], THE was observed in the Bi intercalated Cr_2Te_3 thin film system, which is possible evidence of magnetic skyrmions. However, the Bi nanosheets were inserted into a Cr_2Te_3 thin film, so the interface between Bi and Cr_2Te_3 was not large or uniform. The pure interface of Bi layers and Cr_2Te_3, suitable for mechanism research and future device fabrication, has not been studied yet. The growth scheme of Bi on Cr_2Te_3 layers and the properties of Bi/Cr_2Te_3 heterostructure thin films are still blank.

In this work, Bi/Cr_2Te_3 heterostructure thin films have been grown using molecular beam epitaxy (MBE). The structure of Bi layers grown on hexagonal Cr_2Te_3 (0 0 0 1) surface was revealed to be rectangular Bi (1 1 0) plane by cross-sectional and plane-view transmission electron microscopy (TEM). The signals of THE in the magnetoelectronic transport data, humps and dips near the coercive field, were observed in the Bi/Cr_2Te_3 heterostructure system. The minor-loop method was applied to exclude the possibility of two-component anomalous Hall effect (AHE) that might generate similar hump and dip signals. Moreover, the signals of THE did not vanish until 130 K. The temperature above liquid nitrogen provide feasibility to the following observation of magnetic skyrmions by Lorentz transmission electron microscopy (LTEM).

2. Experimental methods

The Bi/Cr_2Te_3 heterostructure thin film was deposited on intrinsic GaAs (1 1 1) substrates by MBE. Before growth, a piece of undoped GaAs (1 1 1) substrate was heated to 580℃ for deoxidation. After deoxidation, the temperature of the substrate

was decreased to 240 ℃, and the ZnSe source was increased to 760 ℃. The ZnSe buffer layer was deposited on the substrate for 30 minutes. Later, Cr (99.999%) and Te (99.999%) sources were deposited simultaneously on the ZnSe buffer layer. The Cr source was set to 1160 ℃, and the Te source was set to 350 ℃ to keep the flux ratio of 1:10. The flux of Te is much larger than Cr because Te is easily volatilized under vacuum atmosphere[18]. After 1 hour of Cr_2Te_3 growth, the sample temperature was set to room temperature for Bi growth. Then, the Bi (99.995%) source was increased to 500 ℃ and deposited on the Cr_2Te_3 surface. At last, ZnSe with a source temperature of 760 ℃ was capped on the thin film surface at the same temperature to prevent the thin film sample from oxidation. Samples with different Bi growth times were prepared.

This work utilized the FEI Helios 600i focus ion beam (FIB) to prepare cross-sectional and plane-view TEM samples. The preparation method of the plane-view TEM sample in FIB was sketched in supporting information (**Figure S1**). Titan Themis G2 TEM with Double C_s correctors and Talos F200X G2 TEM were used in this work to observe the atomic level images of the interface and characterize crystal structures of thin film samples.

Six-terminal Hall-bar electrodes were prepared using photolithography on the thin film sample. A physical property measurement system (PPMS) measured the magnetoresistance and Hall resistance. PPMS used in this work is from Quantum Design company and can provide a magnetic field of 14 T and a low-temperature environment from 1.9 K to 310 K.

3. Results and Discussion

3.1. Structure characterization

The Bi/Cr_2Te_3 heterostructure thin films were grown on GaAs substrate with the ZnSe layer buffered by the MBE method (details in the experimental methods section). The growth scheme was plotted in **Figure 1a** and the top ZnSe layer was capped to protect the thin film from oxidation. The Bi/Cr_2Te_3 heterostructure thin films with different thickness of the Bi layers were prepared (details in supporting information

Table S1) by changing the growth time. The reflective high energy electron diffraction (RHEED) patterns of one typical sample (the growth time of Bi is 2 hours) were shown in **Figure 1b**. The long streaky lines of Cr_2Te_3 represent high-quality and single-crystal Cr_2Te_3 thin film. The spotty lines of the Bi layer indicated the island growth of Bi. Two sets of line systems were observed in the RHEED pattern of Bi, suggesting rotation domains exist in the Bi layer. XRD was performed on the sample to characterize the crystalline structure, and the spectrum (**Figure S2**) shows that the Cr_2Te_3 layer was grown on the GaAs (1 1 1) substrate in the direction of [0 0 0 1]. The signal of the Bi peak was more and more obvious as the thickness of Bi increases.

The cross-sectional structure of the Bi/Cr_2Te_3 heterostructure samples were observed by scanning transmission electron microscopy (STEM), and the results are shown in **Figures 1c-1f**. The overview of ZnSe/Bi/Cr_2Te_3/ZnSe heterostructure was shown in **Figure 1c**. Bi was grown for 2 hours in this sample and its Energy Dispersive X-Ray (EDX) mapping is displayed in **Figure S4a**. The EDX also claimed that the atomic ratio of Cr:Te is close to 2:3 (**Figure S4b**). The Bi islands were separated on the Cr_2Te_3 layer, which was consistent with spotty RHEED pattern of Bi. Zooming in the interface between Bi and Cr_2Te_3 layers, the demonstrated side-view crystalline structure of Bi (1 1 0) surface and Cr_2Te_3 (0 0 0 1) surface (details in **Figure S3**) was coincident with the atomic structure in STEM image as **Figure 1d** indicates. When the growth time of Bi layer increases, some defects appeared in the Bi/Cr_2Te_3 interface as **Figure 1e** shows. The EDX mapping of this sample with 8-hour Bi (**Figure S4c**) exhibits that the thickness of Bi layer is about 70 nm. The atomic structure of Bi layer in **Figure 1f** is similar to **Figure 1d**, which means that the thickness of Bi layer on Cr_2Te_3 surface did not affect the phase of Bi. The arrangement of Bi atoms fits well with the side view (view from $[\bar{1}\ 1\ 1]$ direction) of Bi (1 1 0) plane. The layer distance measured from **Figure 1f** is about 0.339 nm, close to the single-layer terrace height of the Bi (1 1 0) surface measured in STM[19].

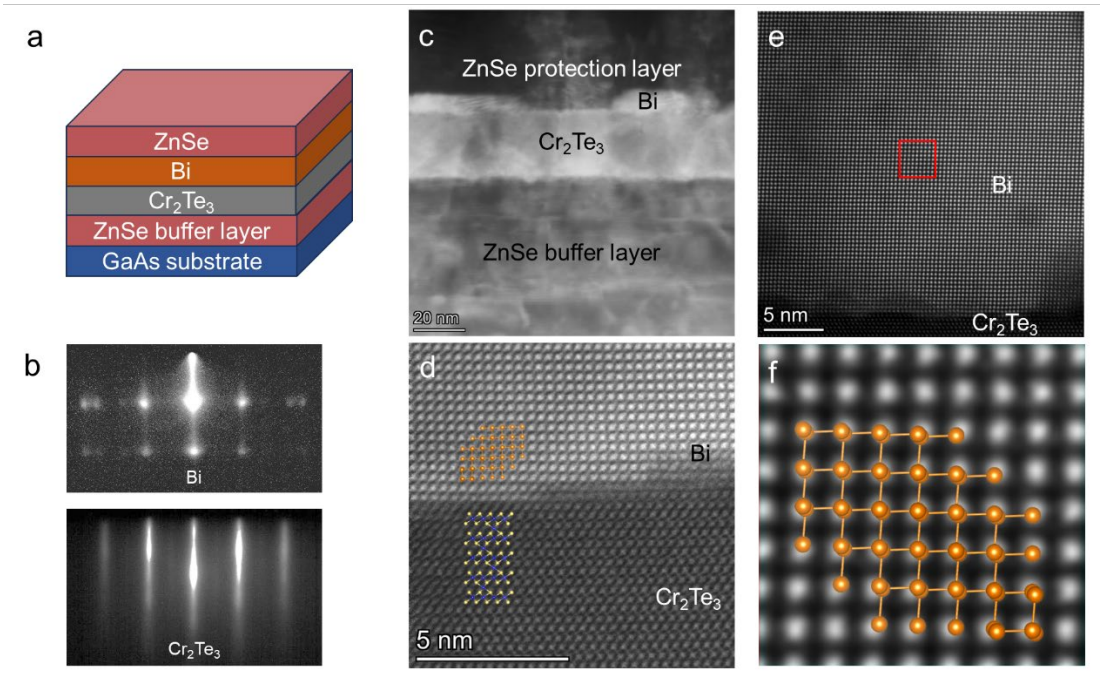

Figure 1. a) Growth scheme of ZnSe/Bi/Cr_2Te_3/ZnSe/GaAs heterostructure thin film. b) Typical RHEED patterns of Cr_2Te_3 layer and Bi layer, the growth time of Bi layer is 2 hours in the sample. c) Cross-sectional STEM image of an overview of ZnSe/Bi/Cr_2Te_3/ZnSe heterostructure thin film, the growth time of Bi layer is 2 hours in the sample. d) Atomic-level Bi/Cr_2Te_3 interface zooming in **Figure 1c**, the Cr_2Te_3 is viewed from the $[0\,1\,\bar{1}\,0]$ direction and the Bi was viewed from the $[\bar{1}\,1\,1]$ direction. e) Cross-sectional STEM image of the Bi/Cr_2Te_3 interface, the growth time of Bi layer is 8 hours in the sample. f) Atomic-level Bi layer zooming in red square area in **Figure 1e**, the arrangement of Bi atoms fits well with the side view (view from $[\bar{1}\,1\,1]$ direction) of Bi (1 1 0) plane.

To better investigate the distribution of Bi islands and atomic structure of Bi layers, plane-view observation would be helpful. An easy method of preparing plane-view thin-film TEM samples by focus ion beam (FIB) was developed in this work (details in experimental methods section). The plane-view STEM images of the Bi/Cr_2Te_3 heterostructure thin film samples were shown in **Figure 2** and the corresponding EDX mapping were shown in **Figure S5**. The large-scale images (**Figure 2a-2c**) revealed that the increased growth time (2 hours-8 hours) of Bi layer enlarged the size and

density of the Bi islands. As the growth time of Bi increased, the isolated islands grew gradually, connected with other islands nearby, and the vacancies between islands became narrower and narrower until some small islands converged into large islands. The average domain size linearly depends on the average thickness of Bi (Figure S6). However, the density of Bi islands might not increase monotonically as the coverage of Bi islands increases due to the coalescence of Bi islands at the beginning[20].

In the Bi/Cr_2Te_3 sample with 2-hour Bi, as **Figure 2a** shows, the average size of one Bi island is about 20×60 nm, and the distance between the two nearest islands is about 20 nm. The rectangle-shaped Bi islands are distributed on the surface randomly without preference for elongated direction. The plane-view STEM of Bi islands with different orientations coincides with the double lines in the Bi RHEED pattern. The quasi-square lattice is presented clearly from the atomic-level plane-view STEM images shown in **Figure 2d** and **2e**. In addition, the estimated length and width of a unit cell are 0.477 nm (+ 0.42 %) × 0.473 nm (+ 4.19 %), which is approximately equal to the unit cell values in the Bi (1 1 0) plane[21]. The calculated Bi crystal structure in the (1 1 0) facet fits well on the atomic-level STEM image as **Figure 2e** shows. When the growth time of Bi layer increased to 8 hours, the structure of Bi still kept quasi-square lattice as **Figure 2f** and **2g** shows. However, the lattice constants changed into 0.479 nm (+ 0.84 %) × 0.461 nm (+ 1.54 %). The lattice constants of thicker Bi were closer to the intrinsic Bi (1 1 0) surface[21].

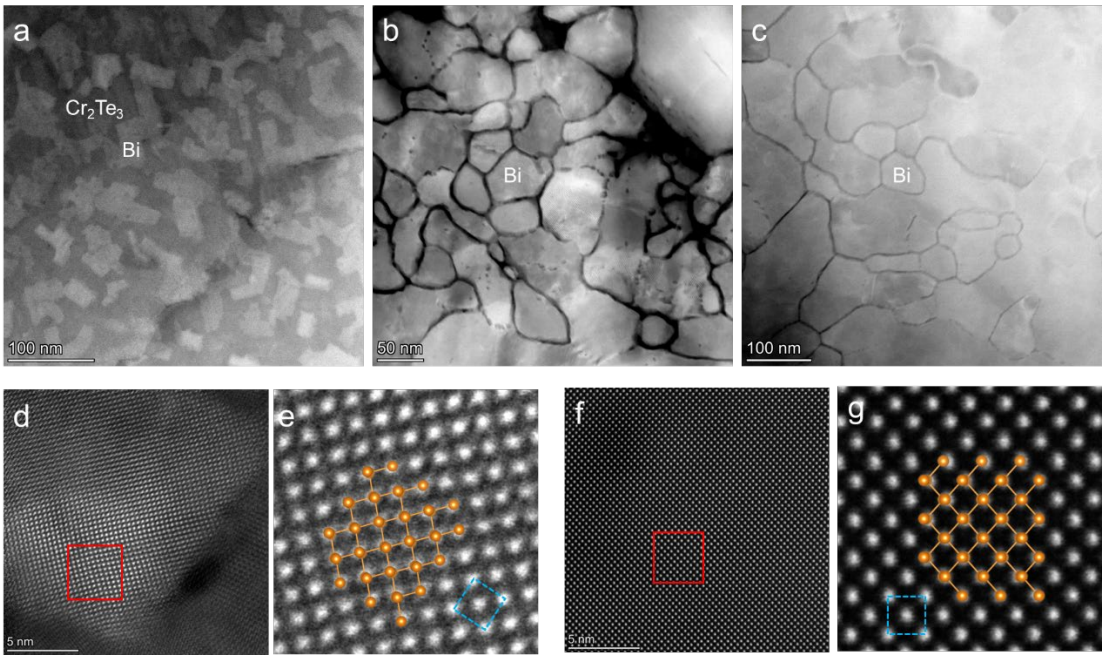

Figure 2. a) Large-scale plane-view texture of Bi islands grown for 2 hours. b) Large-scale plane-view texture of Bi layer grown for 5 hours. c) Large-scale plane-view texture of Bi layer grown for 8 hours. d) Plane-view image of one Bi island in **Figure 2a**. e) Atomic-level Bi structure zooming in red square area in **Figure 2d**, the estimated length and width of a unit cell (blue dash rectangle) are 0.477 nm (+ 0.42 %) × 0.473 nm (+ 4.19 %). f) Zoom-in plane-view image of the Bi layer in **Figure 2c**. g) Atomic-level Bi structure zooming in red square area in **Figure 2f**, the estimated length and width of a unit cell (blue dash rectangle) are 0.479 nm (+ 0.84 %) × 0.461 nm (+ 1.54 %). The arrangement of Bi atoms is consistent with the Bi (1 1 0) surface.

Although Cr_2Te_3 (0 0 0 1) below Bi layer is a hexagonal lattice, Bi grows in a quasi-square lattice along [1 1 0] direction, rather than following a hexagonal lattice along [1 1 1] direction. Both of Bi (1 1 0) and Bi (1 1 1) phase were observed on ferromagnetic hexagonal Fe_3GeTe_2 substrate and Bi (1 1 0) phase would dominate when the coverage of Bi layer increases[22]. But only Bi (1 1 0) single phase was observed on Cr_2Te_3 surface. Previous research had reported that Bi (1 1 0) thin film would transform into Bi (1 1 1) structure when Bi (1 1 0) is over a critical thickness: 4 monolayers (ML)[23]. However, the orientation of the Bi thin film in this work did not change from (1 1 0) into (1 1 1) even though the thickness of Bi thin film is over 70 nm (8 hours). Another calculation

and experiment revealed that the critical thickness of Bi structural transition on Si (1 1 1) substrate is related to growth rate, and a lower growth rate yields a larger value of critical thickness[24]. The growth rate of Bi layer on Cr_2Te_3 surface is approximately equal to 0.429 ML/min. The critical thickness of Bi structural transition on Si (1 1 1) 7×7 substrate under 0.47 ML/min growth rate is 9 ML[19]. However, the critical thickness of Bi structural transition on Cr_2Te_3 layer under a similar growth rate is much larger than on Si (1 1 1) 7×7 substrate.

3.2 Electronic transport properties

The Bi/Cr_2Te_3 heterostructure samples were fabricated into a Hall-bar device before transporting into the PPMS chamber. **Figure 3a** illustrates the schematic of the device and measurement. The external magnetic field was applied perpendicular to the sample surface. In this section, the experimental data was measured in the Bi/Cr_2Te_3 heterostructure thin film that the growth time of Bi is 2 hours. **Figure 3b** shows the R-T curve of this sample. It presents an inflection point due to the ferromagnetic-paramagnetic transition of Cr_2Te_3. The transition temperature is about 170 K, which is close to the Curie temperature (T_C) of this sample (**Figure S7a**). **Figure 3c** shows the Hall-bar device fabricated by the photolithography method. The magneto resistivity (ρ_{xx}) loop of the Bi/Cr_2Te_3 sample under a sweeping perpendicular magnetic field (B) at different temperatures was measured (**Figure S8**). At the temperature below T_C, the shape of curves behaves like a butterfly, which is typical for ferromagnets with PMA[25].

Previous experiments revealed that the THE signals could emerge in Bi intercalated Cr_2Te_3 thin films[16]. In principle, THE signal will also be observed in the Bi/Cr_2Te_3 heterostructure thin films, and the Hall resistivity measurements will assist in proving it. **Figure 3d** presents the Hall resistivity (ρ_{xy}) of the Bi/Cr_2Te_3 sample when sweeping the perpendicular magnetic field (B) back and forth from 10 K to 150 K. At the temperature below 130 K, the square hysteresis due to anomalous Hall effect (AHE) and PMA of Cr_2Te_3 are observed. In addition, humps and dips, that are evidence of

THE, appear near the coercive field. **Figure S9** shows the ρ_{xy}-B curves of Cr_2Te_3 thin film sample, without Bi layer, grown under the same condition. The humps and dips were not observed at 40 K, 70 K, 95 K. In addition, previous research also reported that only AHE loop without THE signals can be observed in Cr_2Te_3 thin film[26]. Thus, the humps and dips in ρ_{xy}-B curves of Bi/Cr_2Te_3 thin film were probably related to the interface between Bi and Cr_2Te_3. The signals still exist even though the AHE sign becomes opposite at 130 K. At 150 K close to the T_C of Cr_2Te_3, the AHE loop nearly vanishes.

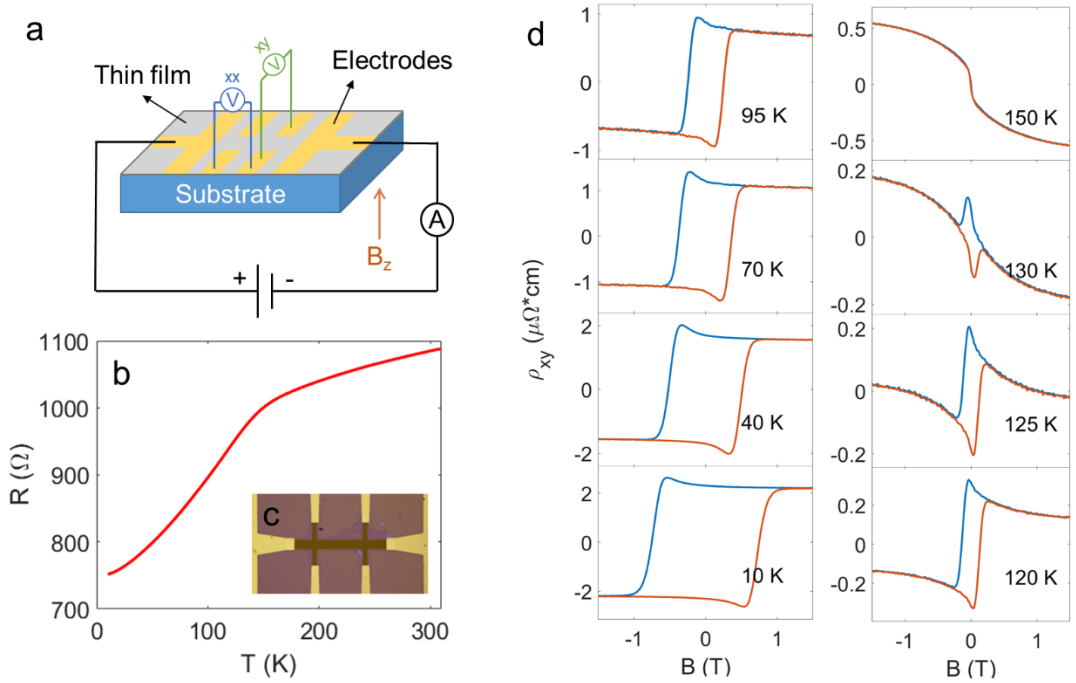

Figure 3. a) Schematic of Hall bar device used in PPMS measurement. b) R-T curve of Bi/Cr_2Te_3 sample. c) Optical microscope photo of the Hall bar device. d) ρ_{xy}-B curves of Bi/Cr_2Te_3 sample at different temperatures. The humps and dips, that are evidence of THE, appear near the coercive field below 140 K. The red (blue) curves were measured by decreasing (increasing) the magnetic field.

The hump and dip in the vicinity of the coercive field could be induced by either THE or two-component AHE, as **Figure 4a** illustrates. The hump and dip signals might also be the superposition of AHE with two opposite signs. Some researchers observed THE-like signals in transport results, but they turned out to be two-component AHE rather than genuine THE[27-30]. Some methods exist to distinguish them, such as temperature

dependence and minor loop[31]. If the hump and dip signals were due to the superposition of AHE and THE, the THE resistivity from 40 K to 95 K has been calculated and plotted in **Figure 4b**. It was calculated by $\rho_{THE} = \rho_{xy} - \rho_0 B - 4\pi\rho_s M$, where ρ_{xy} is measured Hall resistivity, ρ_0 and ρ_s are two different constants and M is the magnetization. The magnetization of the sample has been measured and shown in **Figure S7b**. The following minor-loop experiment will assist to clarify that the hump and dip signals in the Bi/Cr_2Te_3 heterostructure thin film sample emerged by THE rather than two-component AHE.

A minor loop method was performed on this Bi/Cr_2Te_3 sample at 40 K and 70 K. The experimental results are shown in **Figure 4c** and **4d**. In the full loop, the external perpendicular magnetic field was applied to 2 T to polarize the spins in the sample completely. Then, the Hall resistance was measured while sweeping the magnetic field in the sequence of 2 T → -2 T → 2 T. In the minor loop, a 2 T magnetic field was applied first, and then the Hall resistance was measured while sweeping the magnetic field in the sequence of 2 T → $B_{n\text{-}max}$ → 2 T, where $B_{n\text{-}max}$ is the negative maximum magnetic field during measurement. In **Figure 4c and 4d**, the $B_{n\text{-}max}$ is 0 T, -0.2 T, -0.5 T, and -1 T, respectively. If the hump and dip were generated by two-component AHE, the measured loop would highly depend on the $B_{n\text{-}max}$, the value and corresponding magnetic field of maximum R_{xy} vary as $B_{n\text{-}max}$ changes[31, 32]. However, the raw data of minor loop measurement shown in **Figure 4c** and **4d** display the nearly overlapping minor loops and the hump and dip appear at the same positions regardless of $B_{n\text{-}max}$, as the dash lines indicated. It means that THE is probably the reason for emerging the humps and dips near the coercive field. In **Figure 4c**, the R_{xy}-B loop in which the $B_{n\text{-}max}$ is -0.5 T does not repeat the full loop, but the position where the dip appears is the same as the other loops, as the gray dashed line indicates. The $B_{n\text{-}max}$ of -0.5 T is not large enough for the spins in a thin film to reverse direction completely, so a smaller coercive field is sufficient when sweeping the magnetic field back.

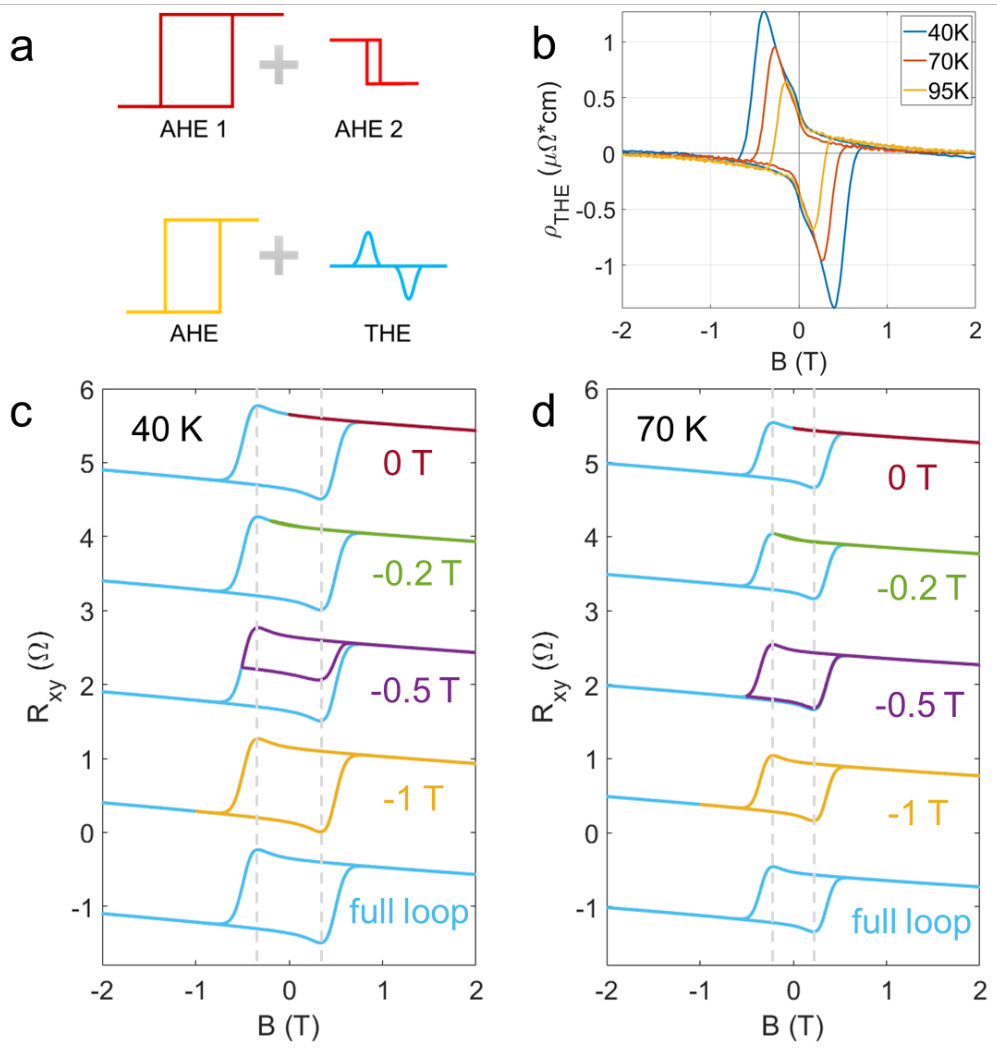

Figure 4. a) Illustration of two mechanisms that might generate hump and dip near the coercive field: two-component AHE with opposite signs or the superposition of AHE and THE. b) THE resistivity of Bi/Cr_2Te_3 sample at 40 K, 70 K, 95 K. c) Full loop ($B_{n\text{-}max}$ = -2 T) and minor loops at 40 K with magnetic field stopping at -1 T, -0.5 T, -0.2 T and 0 T. d) Full loop ($B_{n\text{-}max}$ = -2 T) and minor loops at 70 K with magnetic field stopping at -1 T, -0.5 T, -0.2 T and 0 T.

THE signals could be affected by plenty of factors including chemical compositions, thickness, interface, strain and defects[3]. The quality of Bi/Cr_2Te_3 interface and the thickness of Bi layer influence the intensity of THE in the Bi/Cr_2Te_3 heterostructure thin films (details in supporting information **Figure S10**). THE is important evidence for the existence of magnetic skyrmions and the persisted temperature of THE signals in the Bi/Cr_2Te_3 heterostructure thin film was increased to

130 K compared with the previous 70 K in Bi-intercalated Cr_2Te_3 samples[17]. The higher THE temperature in Bi/Cr_2Te_3 heterostructure thin films allowed magnetic skyrmions observation by Lorentz transmission electron microscope (LTEM) at liquid nitrogen temperature. Therefore, LTEM was performed in the Bi/Cr_2Te_3 heterostructure thin film. Some specious bubbles were observed in the samples and the contrast was reversed in the under-focus and over-focus images (details in supporting information **Figure S11**). They look like the magnetic skyrmions reported in previous research[7, 33]. Whether the bubbles were magnetic skyrmions still needs more solid evidence. However, the size of these bubbles (dozens of nanometers) is comparable with the resolution of LTEM (6 nm), so the reconstruction directly from LTEM images seems impossible. Other technology (such as spin-resolved STM and 4D STEM) with higher resolution would be helpful to investigate the spin texture of these bubbles and clarify the existence of magnetic skyrmions.

The magneto transport properties of thin films might be affected by the substrate[34]. Therefore, the Bi/Cr_2Te_3 heterostructure could be grown on different substrates in future to investigate the influence of substrates. Besides, the heterostructures of Bi and other Cr-Te compounds with PMA at room temperature (such as $CrTe_2$[35, 36]) could be prepared by a similar growth scheme in the following research, which might be a new approach to produce room-temperature magnetic skyrmions. Besides, the controllable interface between Bi and Cr-Te compounds makes it possible to fabricate spintronic devices for future applications.

4. Conclusion

Bi/Cr_2Te_3 heterostructure thin film samples have been prepared on GaAs (1 1 1) substrates with ZnSe buffered. The cross-sectional and plane-view STEM images displayed the island growth of the square Bi (1 1 0) layer on Cr_2Te_3 (0 0 0 1) surface, and Bi (1 1 0) structure did not transform to Bi (1 1 1) even over 70 nm. As the growth time of Bi increases, the Bi islands grow up and connect with islands nearby to form larger islands. PPMS results exhibited hump and dip signals near the coercive field in

Bi/Cr_2Te_3 heterostructure thin films below 130 K. Another possible origin of the similar signals, two-component AHE, has been ruled out by the minor loop experimental results. The higher THE temperature provided feasibility for magnetic skyrmions observation by LTEM or spin-polarized STM at liquid nitrogen temperature in the future.

References

(1) Bruno, P.; Dugaev, V.; Taillefumier, M. Topological Hall effect and Berry phase in magnetic nanostructures. *Physical review letters* **2004**, *93* (9), 096806.

(2) Berry, M. V. Quantal phase factors accompanying adiabatic changes. *Proceedings of the Royal Society of London. A. Mathematical and Physical Sciences* **1984**, *392* (1802), 45-57.

(3) Wang, H.; Dai, Y.; Chow, G.-M.; Chen, J. Topological hall transport: Materials, mechanisms and potential applications. *Progress in Materials Science* **2022**, *130*, 100971. DOI: 10.1016/j.pmatsci.2022.100971.

(4) Laha, A.; Singha, R.; Mardanya, S.; Singh, B.; Agarwal, A.; Mandal, P.; Hossain, Z. Topological Hall effect in the antiferromagnetic Dirac semimetal EuAgAs. *Physical Review B* **2021**, *103* (24), L241112. DOI: 10.1103/PhysRevB.103.L241112.

(5) Shiomi, Y.; Iguchi, S.; Tokura, Y. Emergence of topological Hall effect from fanlike spin structure as modified by Dzyaloshinsky-Moriya interaction in MnP. *Physical Review B* **2012**, *86* (18), 180404. DOI: 10.1103/PhysRevB.86.180404.

(6) Wu, Y.; Zhang, S.; Zhang, J.; Wang, W.; Zhu, Y. L.; Hu, J.; Yin, G.; Wong, K.; Fang, C.; Wan, C.; et al. Neel-type skyrmion in WTe2/Fe3GeTe2 van der Waals heterostructure. *Nat Commun* **2020**, *11* (1), 3860. DOI: 10.1038/s41467-020-17566-x From NLM PubMed-not-MEDLINE.

(7) Ding, B.; Li, Z.; Xu, G.; Li, H.; Hou, Z.; Liu, E.; Xi, X.; Xu, F.; Yao, Y.; Wang, W. Observation of Magnetic Skyrmion Bubbles in a van der Waals Ferromagnet

Fe(3)GeTe(2). *Nano Lett* **2020**, *20* (2), 868-873. DOI: 10.1021/acs.nanolett.9b03453 From NLM PubMed-not-MEDLINE.

(8) T.H.R.Skyrme. A unified field theory of mesons and baryons. *Nuclear Physics* **1962**, *31*, 14. DOI: 10.1016/0029-5582(62)90775-7.

(9) Rossler, U. K.; Bogdanov, A. N.; Pfleiderer, C. Spontaneous skyrmion ground states in magnetic metals. *Nature* **2006**, *442* (7104), 797-801. DOI: 10.1038/nature05056 From NLM PubMed-not-MEDLINE.

(10) Nagaosa, N.; Tokura, Y. Topological properties and dynamics of magnetic skyrmions. *Nat Nanotechnol* **2013**, *8* (12), 899-911. DOI: 10.1038/nnano.2013.243 From NLM Medline.

(11) Li, B.; Deng, X.; Shu, W.; Cheng, X.; Qian, Q.; Wan, Z.; Zhao, B.; Shen, X.; Wu, R.; Shi, S.; et al. Air-stable ultrathin Cr3Te4 nanosheets with thickness-dependent magnetic biskyrmions. *Materials Today* **2022**, *57*, 66-74. DOI: 10.1016/j.mattod.2022.04.011.

(12) Chen, Y.; Zhu, Y.; Lin, R.; Niu, W.; Liu, R.; Zhuang, W.; Zhang, X.; Liang, J.; Sun, W.; Chen, Z.; et al. Observation of Colossal Topological Hall Effect in Noncoplanar Ferromagnet Cr5Te6 Thin Films. *Advanced Functional Materials* **2023**, *33* (33), 2302984. DOI: https://doi.org/10.1002/adfm.202302984.

(13) Liu, J.; Ding, B.; Liang, J.; Li, X.; Yao, Y.; Wang, W. Magnetic Skyrmionic Bubbles at Room Temperature and Sign Reversal of the Topological Hall Effect in a Layered Ferromagnet Cr0.87Te. *ACS Nano* **2022**, *16* (9), 13911-13918. DOI: 10.1021/acsnano.2c02928.

(14) Zhao, D.; Zhang, L.; Malik, I. A.; Liao, M.; Cui, W.; Cai, X.; Zheng, C.; Li, L.; Hu, X.; Zhang, D.; et al. Observation of unconventional anomalous Hall effect in epitaxial CrTe thin films. *Nano Research* **2018**, *11* (6), 3116-3121. DOI: 10.1007/s12274-017-1913-8.

(15) Zhang, X.; Ambhire, S. C.; Lu, Q.; Niu, W.; Cook, J.; Jiang, J. S.; Hong, D.; Alahmed, L.; He, L.; Zhang, R.; et al. Giant Topological Hall Effect in van der Waals Heterostructures of CrTe2/Bi2Te3. *ACS Nano* **2021**, *15* (10), 15710-15719. DOI:

10.1021/acsnano.1c05519.

(16) Zhou, L.; Chen, J.; Chen, X.; Xi, B.; Qiu, Y.; Zhang, J.; Wang, L.; Zhang, R.; Ye, B.; Chen, P.; et al. Topological Hall Effect in Traditional Ferromagnet Embedded with Black-Phosphorus-Like Bismuth Nanosheets. *ACS Appl Mater Interfaces* **2020**, *12* (22), 25135-25142. DOI: 10.1021/acsami.0c04447 From NLM PubMed-not-MEDLINE.

(17) Chen, J.; Wang, L.; Zhang, M.; Zhou, L.; Zhang, R.; Jin, L.; Wang, X.; Qin, H.; Qiu, Y.; Mei, J.; et al. Evidence for Magnetic Skyrmions at the Interface of Ferromagnet/Topological-Insulator Heterostructures. *Nano Lett* **2019**, *19* (9), 6144-6151. DOI: 10.1021/acs.nanolett.9b02191 From NLM PubMed-not-MEDLINE.

(18) Ishibe, T.; Komatsubara, Y.; Ishikawa, K.; Takigawa, S.; Naruse, N.; Mera, Y.; Yamashita, Y.; Ohishi, Y.; Nakamura, Y. Boosting Thermoelectric Performance in Epitaxial GeTe Film/Si by Domain Engineering and Point Defect Control. *ACS Applied Materials & Interfaces* **2023**, *15* (21), 26104-26110. DOI: 10.1021/acsami.3c01404.

(19) Nagase, K.; Kokubo, I.; Yamazaki, S.; Nakatsuji, K.; Hirayama, H. Structure and growth of Bi(110) islands on Si(111)sqrt(3)×sqrt(3)−B substrates. *Physical Review B* **2018**, *97* (19), 195418. DOI: 10.1103/PhysRevB.97.195418.

(20) Peng, X.; Liang, H.; Dong, X.; Yang, H.; Wang, X.; Qiao, L.; Li, J.; Wang, C.; Han, J.; Wang, Q.; et al. Epitaxial growth of Bi(110) and Bi(2)Se(3)thin films on a ferromagnetic insulator substrate of Cr(2)Ge(2)Te(6). *J Phys Condens Matter* **2021**, *33* (41), 415001. DOI: 10.1088/1361-648X/ac1535 From NLM PubMed-not-MEDLINE.

(21) Yaginuma, S.; Nagaoka, K.; Nagao, T.; Bihlmayer, G.; M. Koroteev, Y.; V. Chulkov, E.; Nakayama, T. Electronic Structure of Ultrathin Bismuth Films with A7 and Black-Phosphorus-like Structures. *Journal of the Physical Society of Japan* **2008**, *77* (1), 014701. DOI: 10.1143/jpsj.77.014701.

(22) Xi, Y.; Shi, Z.; Zhao, M.; Cheng, N.; Du, K.; Li, K.; Xu, H.; Xu, S.; Liu, J.; Feng, H.; et al. Modulation of Kondo Behavior in a Two-Dimensional Epitaxial Bilayer Bi(111)/Fe3GeTe2 Moiré Heterostructure. *ACS Nano* **2024**, *18* (34), 22958-22964. DOI: 10.1021/acsnano.4c04271.

(23) Nagao, T.; Sadowski, J. T.; Saito, M.; Yaginuma, S.; Fujikawa, Y.; Kogure, T.; Ohno, T.; Hasegawa, Y.; Hasegawa, S.; Sakurai, T. Nanofilm allotrope and phase transformation of ultrathin Bi film on Si(111)-7x7. *Phys Rev Lett* **2004**, *93* (10), 105501. DOI: 10.1103/PhysRevLett.93.105501 From NLM PubMed-not-MEDLINE.

(24) Ushioda, R.; Shimura, M.; Nakatsuji, K.; Hirayama, H. Growth-rate dependence of the structural transition of bismuth islands on Si(111) substrates. *Physical Review Materials* **2022**, *6* (4), 043403. DOI: 10.1103/PhysRevMaterials.6.043403.

(25) Roy, A.; Guchhait, S.; Dey, R.; Pramanik, T.; Hsieh, C.-C.; Rai, A.; Banerjee, S. K. Perpendicular magnetic anisotropy and spin glass-like behavior in molecular beam epitaxy grown chromium telluride thin films. *ACS nano* **2015**, *9* (4), 3772-3779.

(26) Wen, Y.; Liu, Z.; Zhang, Y.; Xia, C.; Zhai, B.; Zhang, X.; Zhai, G.; Shen, C.; He, P.; Cheng, R.; et al. Tunable Room-Temperature Ferromagnetism in Two-Dimensional Cr(2)Te(3). *Nano Lett* **2020**, *20* (5), 3130-3139. DOI: 10.1021/acs.nanolett.9b05128 From NLM PubMed-not-MEDLINE.

(27) Fijalkowski, K. M.; Hartl, M.; Winnerlein, M.; Mandal, P.; Schreyeck, S.; Brunner, K.; Gould, C.; Molenkamp, L. W. Coexistence of Surface and Bulk Ferromagnetism Mimics Skyrmion Hall Effect in a Topological Insulator. *Physical Review X* **2020**, *10* (1), 011012. DOI: 10.1103/PhysRevX.10.011012.

(28) Cho, S. W.; Lee, I. H.; Lee, Y.; Kim, S.; Khim, Y. G.; Park, S. Y.; Jo, Y.; Choi, J.; Han, S.; Chang, Y. J.; et al. Investigation of the mechanism of the anomalous Hall effects in Cr(2)Te(3)/(BiSb)(2)(TeSe)(3) heterostructure. *Nano Converg* **2023**, *10* (1), 2. DOI: 10.1186/s40580-022-00348-0 From NLM PubMed-not-MEDLINE.

(29) Kan, D.; Moriyama, T.; Kobayashi, K.; Shimakawa, Y. Alternative to the topological interpretation of the transverse resistivity anomalies in SrRuO3. *Physical Review B* **2018**, *98* (18), 180408. DOI: 10.1103/PhysRevB.98.180408.

(30) Zhu, M.; Cui, Z.; Li, W.; Shan, Z.; Wang, J.; Huang, H.; Fu, Z.; Lu, Y. Anomalous Hall effect in spatially inhomogeneous SrRuO3 films. *AIP Advances* **2021**, *11* (12), 125027. DOI: 10.1063/5.0047065 (acccessed 7/15/2023).

(31) Tai, L.; Dai, B.; Li, J.; Huang, H.; Chong, S. K.; Wong, K. L.; Zhang, H.; Zhang,

P.; Deng, P.; Eckberg, C.; et al. Distinguishing the Two-Component Anomalous Hall Effect from the Topological Hall Effect. *ACS Nano* **2022**, *16* (10), 17336-17346. DOI: 10.1021/acsnano.2c08155 From NLM PubMed-not-MEDLINE.

(32) Chi, H.; Ou, Y.; Eldred, T. B.; Gao, W.; Kwon, S.; Murray, J.; Dreyer, M.; Butera, R. E.; Foucher, A. C.; Ambaye, H.; et al. Strain-tunable Berry curvature in quasi-two-dimensional chromium telluride. *Nat Commun* **2023**, *14* (1), 3222. DOI: 10.1038/s41467-023-38995-4 From NLM PubMed-not-MEDLINE.

(33) Yu, X. Z.; Onose, Y.; Kanazawa, N.; Park, J. H.; Han, J. H.; Matsui, Y.; Nagaosa, N.; Tokura, Y. Real-space observation of a two-dimensional skyrmion crystal. *Nature* **2010**, *465* (7300), 901-904. DOI: 10.1038/nature09124 From NLM PubMed-not-MEDLINE.

(34) Alberca, A.; Munuera, C.; Tornos, J.; Mompean, F. J.; Biskup, N.; Ruiz, A.; Nemes, N. M.; de Andres, A.; León, C.; Santamaría, J.; et al. Ferroelectric substrate effects on the magnetism, magnetotransport, and electroresistance of La0.7Ca0.3MnO3thin films on BaTiO3. *Physical Review B* **2012**, *86* (14), 144416. DOI: 10.1103/PhysRevB.86.144416.

(35) Sun, X.; Li, W.; Wang, X.; Sui, Q.; Zhang, T.; Wang, Z.; Liu, L.; Li, D.; Feng, S.; Zhong, S.; et al. Room temperature ferromagnetism in ultra-thin van der Waals crystals of 1T-CrTe2. *Nano Research* **2020**, *13* (12), 3358-3363. DOI: 10.1007/s12274-020-3021-4.

(36) Zhang, X.; Lu, Q.; Liu, W.; Niu, W.; Sun, J.; Cook, J.; Vaninger, M.; Miceli, P. F.; Singh, D. J.; Lian, S. W.; et al. Room-temperature intrinsic ferromagnetism in epitaxial CrTe(2) ultrathin films. *Nat Commun* **2021**, *12* (1), 2492. DOI: 10.1038/s41467-021-22777-x From NLM PubMed-not-MEDLINE.

ASSOCIATED CONTENT

Supporting Information

Additional experimental details and methods

AUTHOR INFORMATION

Corresponding Author

*E-mail: yanzj@sustech.edu.cn

*E-mail: daniel.lau@polyu.edu.hk

*E-mail: wangg@sustech.edu.cn